Earthquake Geotechnical Engineering for Protection and Development of Environment and Constructions – Silvestri & Moraci (Eds)
© 2019 Associazione Geotecnica Italiana, Rome, Italy, ISBN 978-0-367-14328-2

Probabilistic assessment of the earthquake-induced displacements of a slope using finite element analysis

E.M. Rathje & Y. Cho
University of Texas at Austin, Austin, TX, USA

ABSTRACT: Predicting the earthquake-induced permanent displacements of a slope involves significant variabilities, particularly due to the variability in the characteristics of the input ground motions. A probabilistic approach that computes a displacement hazard curve can incorporate the variabilities associated with this analysis, such that a rational assessment of the performance of the slope can be obtained. However, to date, only displacements estimated from sliding block analyses have been used to compute probabilistic displacement hazard curves, despite the fact that nonlinear finite element analysis is becoming the preferred method to evaluate the performance of slopes. This paper extends the probabilistic approach for use with displacements from finite element analyses. We develop slope-specific displacement prediction models using displacements computed by nonlinear finite element analyses. Various models are developed that utilize different ground motion intensity measures in an effort to identify the most statistically efficient models. Finally, sliding displacement hazard curves are generated for the slope using the developed predictive models and the ground motion hazard at a site in Northern California.

1 INTRODUCTION

The sliding displacement for a given critical slip surface has been the parameter of choice for evaluating the seismic performance of slopes. This displacement, defined as the cumulative and downward movement of the sliding mass, typically is predicted from sliding block analyses using the yield acceleration (k_y) of the slope along with an empirical displacement relationship (e.g., Bray and Travasarou 2007; Saygili and Rathje, 2008, Rathje et al. 2011). Commonly the displacements are predicted in a deterministic manner using a single ground motion intensity level and considering either the median or median plus one standard deviation displacement level. More recently, a probabilistic framework has been proposed (e.g., Wang and Rathje 2018, Macedo et al. 2018) to better account for the variabilities associated with the earthquake intensity level and displacement prediction, as well as the uncertainties associated with the engineering characterization of the slope.

To date only empirical displacement models based on sliding block analysis have been incorporated into the probabilistic approach for slope displacement. However, nonlinear finite element analysis is becoming the preferred method to evaluate slope performance because it more fully captures the nonlinear, dynamic response of the slope. Additionally, it does not incorporate the various sliding block assumptions, such as displacements being localized on a single sliding surface and a rigid-perfectly plastic response of the sliding surface. As a result, an improved assessment of the performance of slopes can be provided by integrating the results from nonlinear finite element analyses into the probabilistic approach.

This paper utilizes the results from nonlinear finite elements analyses and the probabilistic framework to evaluate the performance of a slope. The experimental centrifuge slope tested by Malasavage (2010) is used for the analysis. The numerical model is calibrated to the centrifuge model test results and then subjected to over 100 earthquake ground motions to generate a dataset of slope displacements for a range of ground motion intensity levels. These

displacements are used to develop slope-specific displacement prediction models. Various models are developed that utilize different intensity measures in an effort to identify the most statistically efficient models. Finally, sliding displacement hazard curves are generated for the slope using the developed predictive models and the ground motion hazard at a site in Northern California.

2 MODEL SLOPE ANALYZED IN THIS STUDY

The centrifuge model test performed at RPI by Malasavage (2010) was selected to calibrate the nonlinear finite element analysis. The centrifuge test measured the permanent displacement of a clay slope under dynamic loadings. The research by Malasavage (2010) primarily focused on the post-seismic movements of the slope; however, the co-seismic displacement responses during harmonic loading were also recorded and used for the calibration exercise in this paper. The experimental procedure and observations are briefly described below; detailed information can be found in the dissertation of Malasavage (2010).

The Model 2B slope was selected for use in this study because it consisted of a homogeneous slope of kaolinite. The model was constructed in a rigid container box with model-scale dimensions of 53cm (long) × 25cm (width) × 20cm (height) and the test was performed at a centrifugal acceleration of 53 g. The slope in the model (Figure 1) was inclined at 30° with a height of 9.54m in prototype scale. Water was impounded at a height of 8.6m (prototype scale), which is 90% of the total height of the model. The slope was instrumented with embedded accelerometers and pore pressure transducers, and surficial LVDTs that measured displacement parallel to the slope.

The slope was constructed such that it was somewhat over-consolidated and thus would not fail during centrifuge spin-up. The over-consolidation ratio (OCR) profile in the slope was estimated by Malasavage (2010) from the measured water content and void ratio at the end of the test. The data indicated that the material near the slope surface experienced an OCR between approximately 4 and 1.5. The total unit weight of the clay was 16.3kN/m^3 and the shear strength parameters of the clay were measured using isotropically-consolidated, undrained (CIU) triaxial tests performed at effective confining pressures between 240 and 620 kPa. Unfortunately, these stresses are significantly larger than the stresses experienced by the slope in the centrifuge model (generally less than 75 kPa). An S_u/σ'_v ratio approach was used to evaluate the undrained shear strength of the centrifuge slope material from the CIU tests. The average $(S_u/\sigma'_v)_{nc}$ was 0.5 from the CIU tests and this value along with the σ'_v and OCR profiles and a SHANSEP exponent of 0.8 were used to develop a profile of undrained shear strength for the model slope. The resulting profile was discretized into 5 layers (Figure 1) with the thicknesses, σ'_v, OCR, and S_u values listed in Table 1. Although the $(S_u/\sigma'_v)_{nc}$ derived from the CIU data is larger than expected for normally consolidated kaolinite, the S_u profile resulted in a pseudo-static yield acceleration of 0.12 g, which is consistent with the peak ground acceleration at which measureable displacements were obtained in the centrifuge

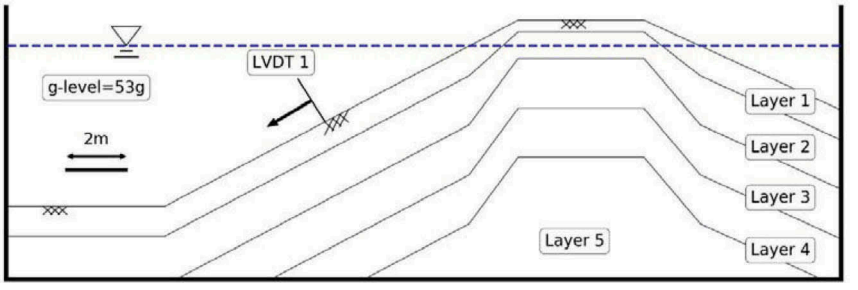

Figure 1. Geometry of model analyzed in this study (prototype scale).

Table 1. Undrained shear strength and shear wave velocity profiles of the kaolinite

Layer No.	Mid Depth (m)	Thickness (m)	σ'_v (kPa)	OCR	S_u (kPa)	Vs (m/s)
1	0.6	1.11	3.5	4.0	5.3	90
2	2.0	1.82	12.6	1.5	8.7	100
3	3.9	1.85	23.9	1.0	12.0	110
4	5.7	1.81	35.3	1.0	17.7	120
5	7.5	1.21	46.6	1.0	23.3	130

model (i.e., between 0.07 and 0.13 g). The shear wave velocity (Vs) of the centrifuge model was measured from the travel time between embedded accelerometers beneath the crest of the model during centrifuge flight (Malasavage 2010). The Vs estimates ranged from 90m/s at a depth of 2m to 140m/s at a depth of 8m (Table 1).

The slope was subjected to a series of sinusoidal and sweep motions at the base of the rigid box. Four sinusoidal motions with peak base accelerations of 0.02g, 0.07g, 0.13g, and 0.44g are used for the validation of the finite element analysis. The nonlinear finite element analysis was performed using the simulation code LS-DYNA (LSTC 2015) as available through the DesignSafe cyberinfrastructure (Rathje et al. 2017). The simulation consisted of a gravitational loading followed by dynamic loading under plane strain condition. In the gravity analysis, the Mohr-Coulomb material model was used with the effective stress strength parameters of c'= 1.4kPa and ϕ'= 31°) obtained from the CIU tests. For the dynamic loading the hysteretic soil model was used with different shear stress-shear strain backbone curves assigned to each layer of the slope based on the effective stress (Table 1). The backbone curves were generated using the GQ/H approach (Groholski et al., 2016), in which the backbone curve follows the modulus reduction curves of Darendeli (2001) up to a shear strain of approximately 0.1% and then approaches a designated target shear strength at larger strains. The final backbone curves were consistent with the shear wave velocities (at small strains) and the undrained shear strengths (at large strains) listed in Table 1. To model the rigid centrifuge container, a prescribed motion boundary condition was used to assign the input motion to the edge and base boundaries of the model. A total stress analysis was adopted for the dynamic loading stage.

The slope-parallel, relative displacement (relative to the base of the centrifuge box) from the LS-DYNA simulation for each input motion was computed by rotating the computed relative horizontal and vertical displacements. The computed slope-parallel displacements at the location of LVDT1 (Figure 1) are compared with those measured in the centrifuge test as a function of the input motion peak ground acceleration (PGA) in Figure 2. The displacements from LS-DYNA are mostly larger than those from the centrifuge test, particularly at the smallest displacement levels, but they have a similar trend of increasing displacements with increasing PGA. Modifying the properties by ± 10% to 20% did not significantly change the LS-DYNA

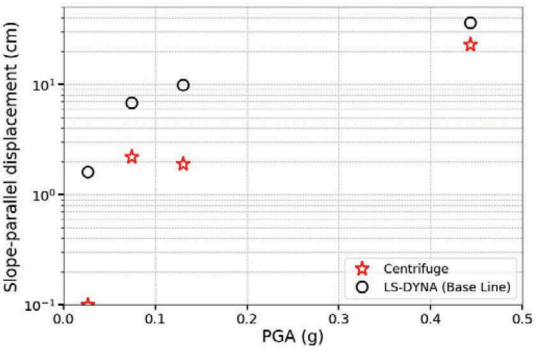

Figure 2. Slope-parallel relative displacements from centrifuge tests and LS-DYNA simulations

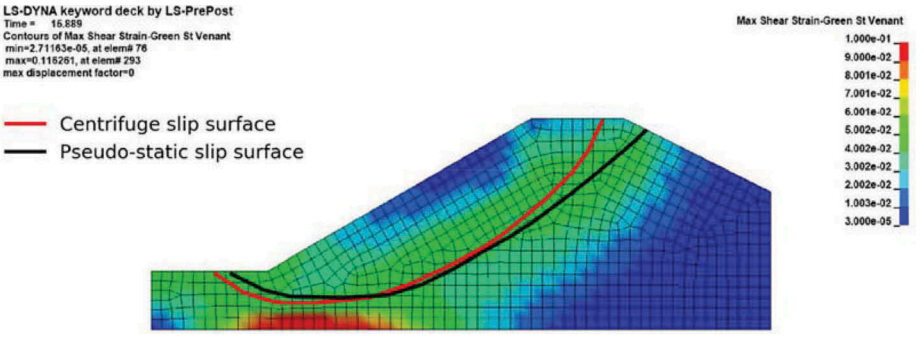

Figure 3. Slip surfaces from centrifuge model and pseudo-static slope stability analysis overlain on maximum shear strains from LS-DYNA analyses.

predictions. There is some uncertainty in the centrifuge measurements because the LVDT was set up to measure only slope-parallel, translational movements and the movements were more rotational. As a result, it is believed that the consistency in displacement trends in Figure 2 provide an adequate calibration of the numerical model. Finally, the slip surfaces from the various approaches of analysis were compared (Figure 3). The centrifuge slip surface was inferred from the final location of the embedded instrumentation (Malasavage 2010) and the pseudo-static slip surface was the critical sliding mass for the computed k_y of 0.122 g. These slip surfaces are shown in Figure 3 along with the maximum shear strain contours computed at the end of shaking from the LS-DYNA simulation for the 0.44g input motion. The slip surfaces are consistent with the localization of shear strain in the LS-DYNA analyses, further demonstrating that the LS-DYNA analyses are capturing the main mechanism of movement in the slope.

3 DEVELOPMENT OF PREDICTIVE MODELS FOR DISPLACEMENT

The variability in the displacement prediction primarily arises from the variability in the input earthquake ground motion, and thus it is important to incorporate a large suite of earthquake ground motions when developing a predictive model for displacement. An important source of input ground motions for shallow crustal earthquakes are available from the NGA-West2 strong motion database of the Pacific Earthquake Engineering Research Center (https://nga west2.berkeley.edu/). A suite of motions was selected from the NGA-West2 database using the following search criteria: earthquake magnitude (M_w) greater than 6.5, closest distance to fault rupture plane (R_{rup}) less than 50km, and average shear wave velocity over the top 30m (Vs30) greater than 500m/s. For each station recording, only the larger component was used for analysis. The resulting suite of motions consisted of 105 time series, 26 of which contained a distinguishable pulse in the time series (i.e., pulse motion) and 89 which did not.

The ground motion characteristics of the different motions are represented in Figure 4 by plotting various ground motion parameters versus the PGA of the motions. Shown in Figure 4 are earthquake magnitude (M_w), peak ground velocity (PGV), Arias intensity (Ia), spectral acceleration at a degraded period of 1.5Ts (Sa(1.5Ts)), where Ts is a fundamental period of the slope and equal to 0.19 s for the critical slip surface of the model slope, mean period (T_m), and pulse period (T_{pulse}). The pulse motions that have directivity effects are shown separately from the non-pulse motions. The PGA of the selected motions range from about 0.03 g to 2 g, consistent with a large range of input intensities. The Ia and Sa(1.5Ts) for the pulse motions are generally consistent with the values for the non-pulse motions, however the PGV and T_m of the pulse motions tend to be larger than the values for the non-pulse motions with similar PGA. The pulse motions have pulse periods generally between 0.5 and 10 s, with most between 5 and 10 s.

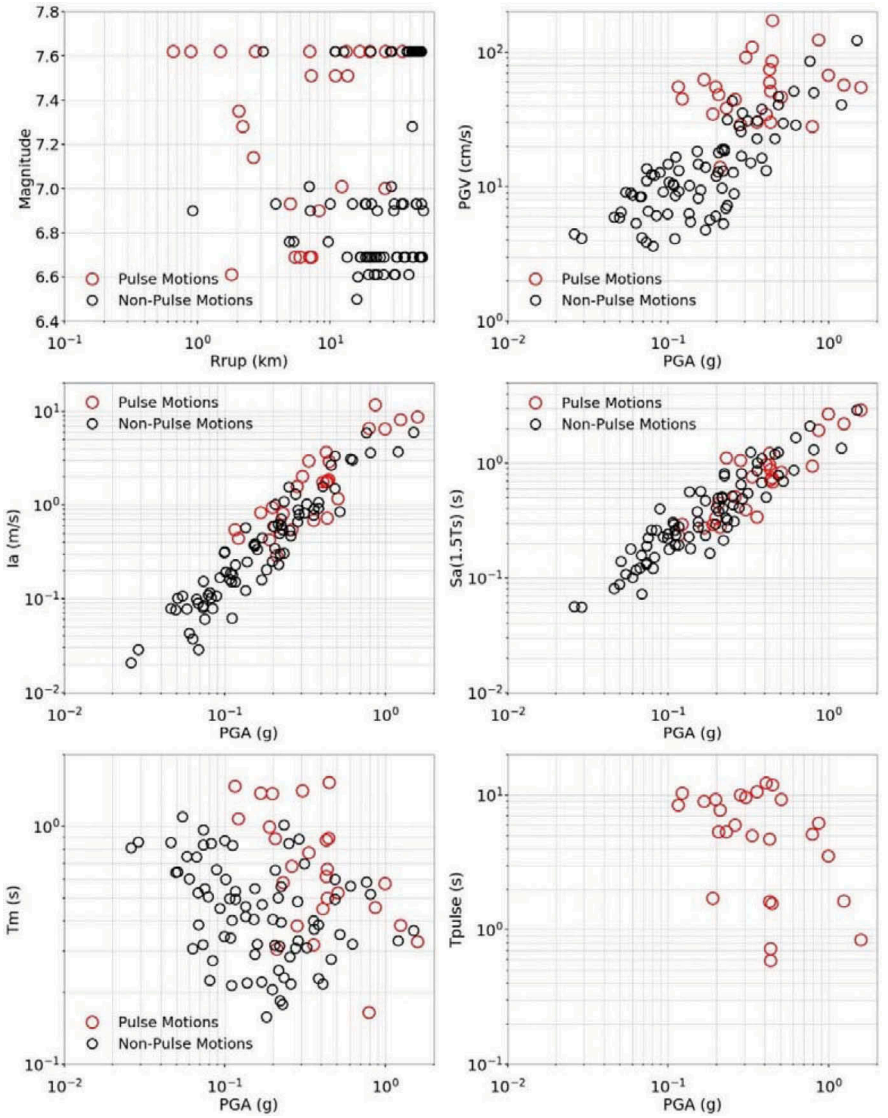

Figure 4. Ground motion characteristics of selected earthquake motions

The displacement models predict the natural log of the displacement (D) as a function of the natural log of one or more ground motion parameters (GM) or earthquake magnitude using one of the following expressions:

$$ln(D) = a0 + a1 \times ln(GM1) \tag{1}$$

$$ln(D) = a0 + a1 \times ln(GM1) + a2 \times (Mw - 7) \tag{2}$$

$$ln(D) = a0 + a1 \times ln(GM1) + a2 \times ln(GM2) \tag{3}$$

where D is displacement in units of cm, $a0$, $a1$, and $a2$ are regression coefficients, GM1 and GM2 are ground motion parameters, and M_w is earthquake magnitude. The value of D from the LS-DYNA simulations was taken as the maximum horizontal displacement along the

surface of the slope. To investigate the efficiency of each of the models (Cornell et al. 2001), the standard deviation of the natural log of the displacement (σ_{ln}) was computed.

Figure 5 plots the computed displacements vs. the five ground motion parameters considered in this study (PGA, PGV, Ia, Sa1.5Ts, and T_m). The data generally show a linear relationship in log-log space for each of the ground motion parameters, and the resulting regression fits and σ_{ln} are shown. For some of the models (e.g., PGA model), the displacements from the pulse motions are generally concentrated above the prediction, while for other models (e.g., PGV model, Ia model) the displacements from the pulse motions are centered around the predictive model. The displacement models that better predict both pulse and non-pulse motions incorporate ground motion parameters that can account for the difference in frequency content between pulse and non-pulse motions and thus separate models for pulse and non-pulse motions are not needed.

The regression parameters for all the models are listed in Table 2. For the single ground motion parameter models shown in Figure 4, the model using Ia displays the smallest

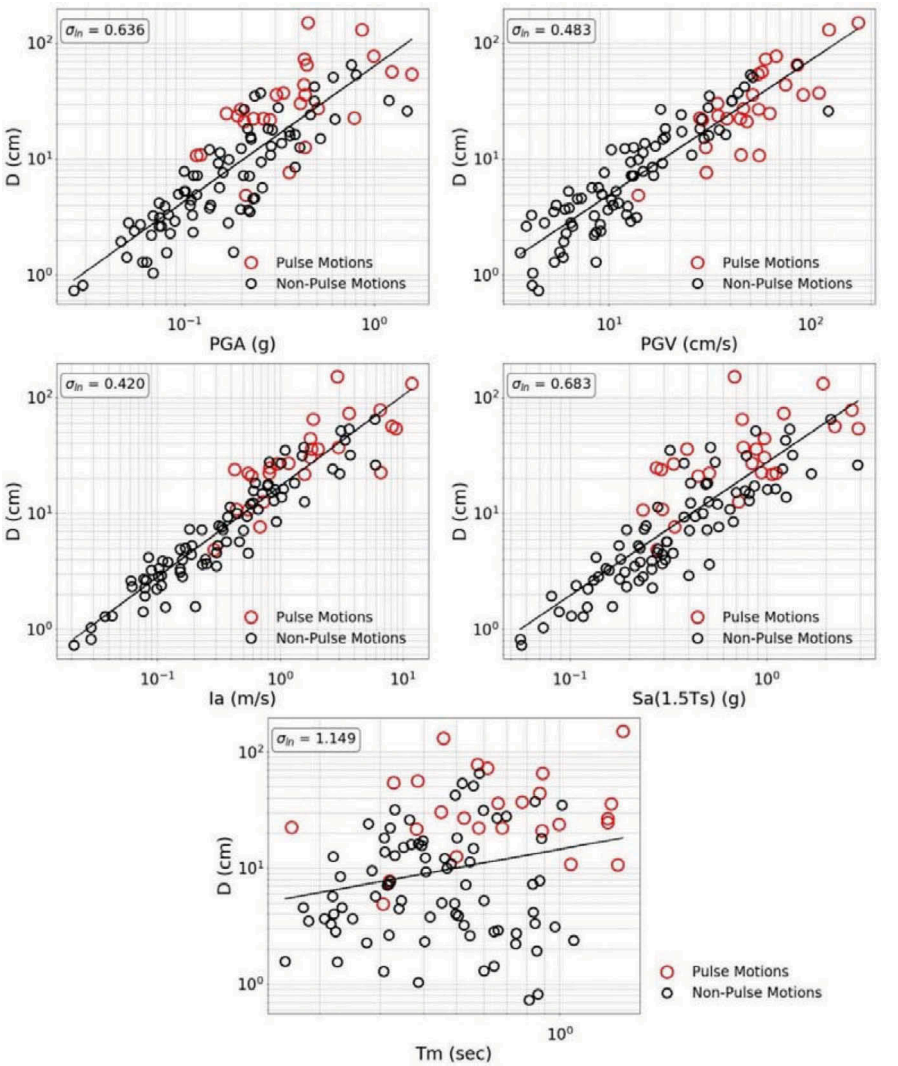

Figure 5. Displacement models that utilize a single ground motion parameter

Table 2. Regression parameters for displacement models using different ground motion parameters

Ground Motion Parameters	$a0$	$a1$	$a2$	σ_{ln}
PGA	4.14	1.16	-	0.636
PGV	-1.09	1.16	-	0.483
Ia	2.83	0.78	-	0.420
Sa(1.5Ts)	3.31	1.15	-	0.683
T_m	2.67	0.53	-	1.149
PGA, M	4.24	1.28	0.84	0.542
PGA, PGV	0.72	0.50	0.82	0.391
PGA, T_m	5.05	1.29	0.97	0.396
PGA, Ia	2.36	-0.39	1.01	0.403
Ia, PGV	1.02	0.48	0.55	0.314
Ia, T_m	3.25	0.79	0.56	0.298

standard deviation (σ_{ln} = 0.42) and is the most efficient of the parameters due to the fact that it captures the three key characteristics of the ground motion: intensity, frequency content, and duration (Saygili et al. 2008). The PGV model has only a slightly larger standard deviation (σ_{ln} = 0.48) and may be more attractive for use because more ground motion models are available to predict PGV than Ia. The PGA and Sa(1.5Ts) models both have σ_{ln} greater than 0.6, and the T_m model has the largest σ_{ln} of 1.15. The larger values of σ_{ln} for the PGA and Sa(1.5Ts) models indicate that these parameters do not adequately capture the frequency content of an earthquake motion. The very large σ_{ln} for the T_m model is not surprising given that it completely ignores ground motion intensity.

Previous studies (e.g., Saygili and Rathje 2008, Rathje and Saygili 2009) have demonstrated that incorporating multiple ground motion parameters can improve the efficiency of displacement prediction models. Thus, models with two ground motion parameters were explored and the regression parameters are shown in Table 2. The simple addition of earthquake magnitude to the PGA model reduces its σ_{ln} by 15% (Table 2), although the σ_{ln} is still larger than for the single parameter models that use either PGV or Ia. A more significant reduction in σ_{ln} is obtained when combining two, complementary ground motion parameters. Combinations that couple either PGA or Ia with other parameters are shown in Figure 6, with the σ_{ln} values for the different models listed in Table 2. The smallest value for σ_{ln} across the models is about 0.3 for both the (Ia, T_m) and (Ia, PGV) models. The other two parameter models (PGA, PGV; PGA, T_m; and PGA, Ia) all have σ_{ln} values around 0.4, which is similar to the value obtained for the single parameter Ia model. The smaller σ_{ln} values associated with the (Ia, T_m) and (Ia, PGV) models indicate that the frequency content information provided by either T_m or PGV helps explain part of the scatter in the displacement data. The similar σ_{ln} values for the (PGA,

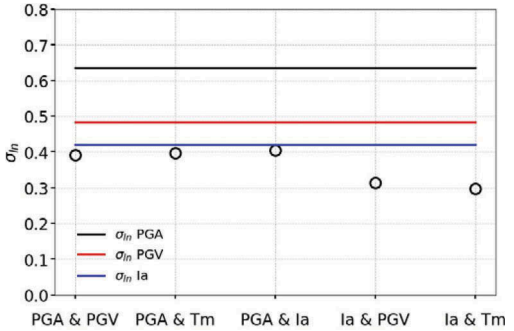

Figure 6. Standard deviation for displacement models using different ground motion parameters

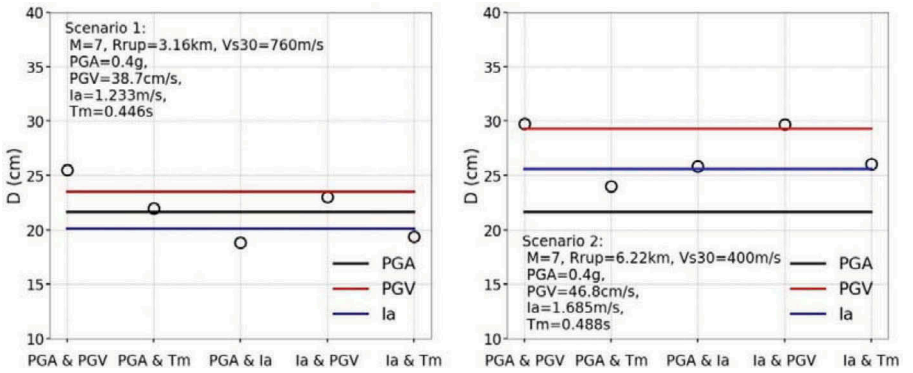

Figure 7. Median displacement predictions from various displacement models for two potential ground motion scenarios

Ia) and Ia models indicates that the intensity information provided by PGA is already captured by Ia and thus the scatter in the data is not reduced by adding PGA.

Based on the comparisons of the σ_{ln} values for the various models, the Ia model is considered the most efficient single parameter displacement model. Importantly, this model has a σ_{ln} that is similar to most of the two parameter models. The most efficient two parameter models are the (Ia, T_m) and (Ia, PGV) models, which display σ_{ln} about 25% smaller than the Ia model. The one issue with using any of these three models is the limited availability of Ia and T_m ground motion models. Of the remaining displacement models, the (PGA, PGV) model is preferred due to the abundance of ground motion models available for PGA and PGV.

An important reason to use displacement models that account for the intensity, frequency content, and duration of motion is to distinguish the shaking characteristics for different soil conditions. Two motions with the same PGA but recorded at sites with different Vs30 will have different values of PGV, Ia, and T_m due to site effects influencing the frequency content and duration of shaking. A displacement model that only includes PGA will not accurately account for these effects on the displacement. To demonstrate this issue two ground motion scenarios for different Vs30 are considered. The first scenario represents an M = 7 event at about 3 km for a site with Vs30 = 760 m/s, and the second scenario represents an M = 7 event at a slightly larger distance of about 6 km for a site with Vs30 = 400 m/s. Both scenarios have PGA = 0.4 g, but the other ground motion parameters are 10% to 40% larger for the Vs30 = 400 m/s scenario. The displacements predicted for the two scenarios using various displacement models are shown in Figure 7. Also misted in Figure 7 are the specific values of PGV, Ia, and T_m for the two scenarios. Obviously, the displacement predicted by the PGA model is the same for the two scenarios because they have the same PGA. However, for all of the other models the displacements increase anywhere from 10% to 40% due to the associated increases in the other ground motion parameters due to site effects. The models that include Ia show the largest increase because Ia was increased the most by the change in Vs30. Note that differences in displacement shown in Figure 7 would have been larger if the ground motions selected as input motions for the analyses had included more motions from sites with smaller Vs30.

4 DISPLACEMENT HAZARD CURVES FOR DIFFERENT DISPLACEMENT MODELS

A seismic displacement hazard curve developed through a probabilistic assessment of sliding displacement (D) computes to the mean annual rate of exceedance (λ_D) for different levels of

the displacement. The computations of λ_D for displacement models incorporating one ground motion parameter (GM), one ground motion parameter and earthquake magnitude (GM, M) and two ground motion parameters ($GM1, GM2$) are given by:

$$\lambda_D(x) = \sum_i P[D>x|GM_i] \times P[GM_i] \tag{4}$$

$$\lambda_D(x) = \sum_i \sum_k P[D>x|GM_i, M_k] \times P[M_k|GM_i] \times P[GM_i] \tag{5}$$

$$\lambda_D(x) = \sum_i \sum_k P[D>x|GM1_i, GM2_k] \times P[GM1_i, GM2_k] \tag{6}$$

where $P[D>x|GM_i]$ is the probability of the displacement exceeding a value of x given ground motion level GM_i and $P[GM_i]$ is the annual probability of occurrence of ground motion level GM_i. $P[D>x|GM_i, M_k]]$ is the probability of the displacement exceeding a value of x given ground motion level GM_i and an earthquake magnitude M_k, and $P[M_k|GM_i]$ is the probability of occurrence of M_k given ground motion level GM_i. $P[M_k|GM_i]$ can be obtained from the hazard disaggregation for GM. $P[D>x|GM1_i, GM2_k]$ is the probability of the displacement exceeding x given the joint occurrence of ground motion levels $GM1_i$ and $GM2_k$, and $P[GM1_i, GM2_k]$ is the joint annual probability of occurrence of ground motion levels $GM1_i$ and $GM2_k$. The details regarding the calculation of each of these components can be found in Rathje et al. (2014).

To demonstrate the displacement hazard curve calculation and compare the results from different models, the ground motion hazard from a site in Northern California (37.75, -122.11) is considered. The PGA hazard curve for Vs30 = 760 m/s and disaggregation for each hazard level were obtained from the USGS Unified Hazard Tool (https://earthquake.usgs.gov/hazards/interactive/) using the Dynamic Conterminous US 2008 (v3.3.1) edition. Of the ground motion parameters investigated in this study (Table 2), hazard curves from the USGS are only available for PGA and thus only models that incorporate PGA are considered. The PGA hazard curve for the site is shown in Figure 8a.

The PGA hazard curve and disaggregation information were used in equations (4) and (5) with the PGA and (PGA, M) models to generate displacement hazard curves. For the (PGA, PGV) displacement model, the Boore et al. (2014) PGA and PGV ground motion models and $\rho_{PGA,PGV} = 0.60$ were used along with the PGA hazard curve and disaggregation to compute the $P[PGA_i, PGV_k]$ information needed for equation (6). These computations were performed

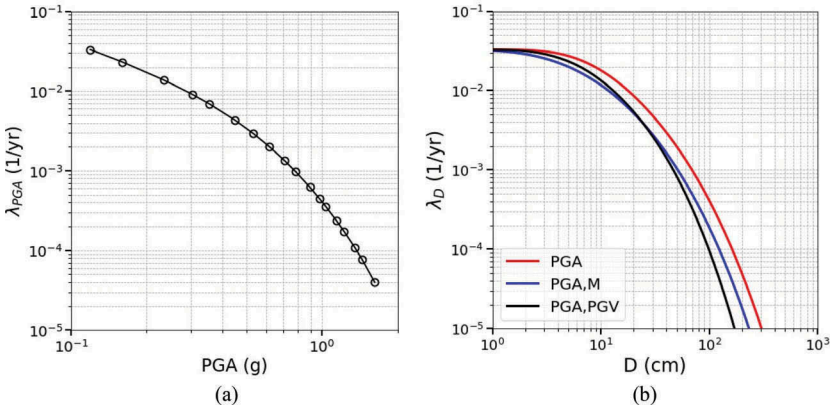

Figure 8. (a) PGA hazard curve for the hypothetical slope location, (b) comparison of hazard curves computed for the PGA, (PGA, M), and (PGA, PGV) displacement models from Table 2.

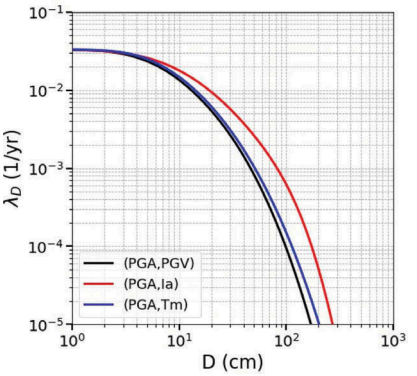

Figure 9. Displacement hazard curves computed for the (PGA, PGV), (PGA, Ia), and (PGV, T_m) displacement models.

in a Jupyter notebook modified from Saygili et al. (2018), which was available on the DesignSafe cyberinfrastructure (www.designsafe-ci.org, Rathje et al. 2017).

The resulting displacement hazard curves for the PGA, (PGA, M), and (PGA, PGV) models are shown in Figure 8b. The PGA model predicts the largest displacements among the three models for various reasons. First, the PGA model has the largest standard deviation (Table 2, Figure 6), which leads to larger displacements contributing to the hazard. Second, the magnitude disaggregation for the site indicates a mean magnitude of about 6.8 and in this magnitude range the PGA model predicts larger displacements than the (PGA, M) model. And finally, neither the PGA nor the (PGA, M) model can explicitly account for frequency content differences that occur due to the effect of site conditions as described by Vs30. It is for all these reasons that a displacement model that incorporate multiple ground motion parameters, such as the (PGA, PGV) model, is recommended for use in displacement analyses.

Of course there are several alternative displacement models that include multiple ground motion parameters. As listed in Table 2, the (PGA, PGV), (PGA, Ia), and (PGV, T_m) models all have similar σ_{ln} and thus, judged on this basis, are all equally optimal options for use in a probabilistic analysis. To assess the potential differences when using these different models, displacement hazard curves were calculated for each model. In computing the required $P[GM1_i, GM2_k]$ for equation (6) for these displacement models, the Travasarou et al. (2003) ground motion model was used for Ia and the Rathje et al. (2004) ground motion model was used for T_m. The relevant correlation coefficients were estimated from Rathje and Saygili (2008) and taken as $\rho_{PGA,Ia} = 0.83$ and $\rho_{PGA,Tm} = -0.27$. The resulting displacement hazard curves are shown in Figure 9. The curves for (PGA, PGV) and (PGA, T_m) are almost indistinguishable, indicating that these two relationships similarly account for frequency content and predict similar relationships for the displacement hazard at this site. Interestingly, the displacement hazard curve for the (PGA, Ia) model predicts the largest displacements. This appears to be caused by the significantly larger standard deviation associated with the Ia ground motion model ($\sigma_{ln} \sim$ 1.0-1.1) relative to other ground motion parameters ($\sigma_{ln} \sim$ 0.5-0.7). As a result, large values of Ia contribute more to the ground motion hazard which leads to larger displacements. The larger standard deviation for Ia has been observed by other researchers (e.g., Campbell and Bozorgnia 2012) and suggests that the difficulty in precisely predicting Ia may make it a less attractive ground motion parameter to use in probabilistic displacement analyses, despite its ability to reduce the standard deviation in the displacement prediction.

5 CONCLUSION

Given the variabilities associated with the prediction of slope displacements induced by earthquake shaking, a displacement hazard curve approach is recommended to evaluate the seismic

performance of slopes. A displacement hazard curve represents the annual rate of exceedance for a range of displacements, computed from the ground motion hazard and a predictive model for slope displacement, and allows for the displacement for a specific annual rate of exceedance to be evaluated. To date, only displacements from sliding block analyses have been used to compute displacement hazard curves, despite the fact that nonlinear finite element analysis is becoming the preferred method to evaluate the movements of slopes. This paper extended the probabilistic approach for use with displacements from finite element analyses and demonstrated its implementation.

An example clay slope, based on the centrifuge work of Malasavage (2010), was used in this study to develop slope-specific displacement models for use in the calculation of the displacement hazard curves. A finite element model of the slope was subjected to over 100 earthquake motions and the computed maximum horizontal displacement for each motion was recorded. These displacements were used to develop predictive models for displacement as a function of one or two ground motion parameters. The Ia displacement model was the one parameter model with the smallest standard deviation (σ_{ln} = 0.42), while the (Ia, PGV) and (Ia, T_m) models had the smallest standard deviation (σ_{ln} ~ 0.3) among the models with two ground motion parameters. The (PGA, PGV), (PGA, Ia), and (PGV, T_m) models have a larger standard deviation (σ_{ln} ~ 0.4) but it is similar to the value for the Ia model.

The developed displacement models were used to compute displacement hazard curves using ground motion hazard information available from the USGS. Of the ground motion parameters considered for the displacement models, hazard curves are only available for PGA, and thus only models that incorporate PGA were used. The displacement models that use a second ground motion parameter to account for frequency content (PGA coupled with PGV, Ia, T_m, or M) generally produce a smaller displacement hazard than models that use PGA alone. Perhaps surprisingly, among these models, the (PGA, Ia) model produces the largest displacement hazard despite the fact that this model has a similar standard deviation to the other models. This result is caused by the significantly larger standard deviation for the Ia ground motion model, which results in larger Ia values being represented in the hazard and generating larger displacements. This result indicates that the variability in both the displacement prediction and the ground motion prediction must be taken into account when evaluating the best displacement models for use in probabilistic analyses.

REFERENCES

Boore, D. M., Stewart, J. P., Seyhan, E. & Atkinson, G. N. 2014. NGA-West2 equations for predicting PGA, PGV, and 5% damped PSA for shallow crustal earthquakes. Earthquake Spectra, 30(3): 1057–1085.

Bray, J. D. & Travasarou, T. 2007. Simplified procedure for estimating earthquake-induced deviatoric slope displacements. Journal of Geotechnical and Geoenvironmental Engineering, 133(4): 381–392.

Campbell, K.W. & Bozorgnia, Y. 2012. A Comparison of ground motion prediction equations for Arias Intensity and Cumulative Absolute Velocity developed using a consistent database and functional form. Earthquake Spectra, 28(3): 931–941.

Cornell C. A. & Luco, N. 2001. Ground motion intensity measures for structural performance assessment at near-fault sites: In Proceedings of the U.S.-Japan joint workshop and third grantees meeting, U.S.-Japan cooperative research on urban earthquake disaster mitigation. Seattle: Washington.

Darendeli, M. B. 2001. Development of a new family of normalized modulus reduction and material damping curves. Ph.D. dissertation, The University of Texas, Austin.

Groholski, D. R., Hashash, Y. M. A., Kim, B., Musgrove, M., Harmon, J. & Stewart J. P. 2016. Simplified model for small-strain nonlinearity and strength in 1D seismic site response analysis. Journal of Geotechnical and Geoenvironmental Engineering, 142(9): doi: 10.1061/(ASCE)GT.1943-5606.0001496.

LSTC, 2015. LS-DYNA keyword user's manual version 971 R8. Livermore Software Technology Corporation, Livermore, California.

Macedo, J., Bray, J., Abrahamson, N. & Travasarou, T. 2018. Performance-based probabilistic seismic slope displacement procedure. Earthquake Spectra, 34(2): 673–695.

Malasavage, N. E. 2010. Post-seismic displacement response in normally consolidated clay slopes. Ph.D. dissertation, Drexel University.

Rathje, E. M., Dawson, C., Padgett, J. E., Pinelli, J. P., Stanzione, D., Adair, A., Arduino, P., Brandenberg, S. J., Cockerill, T., Dey, C., Esteva, M., Haan, F. L.,Jr., Hanlon, M., Kareem, A., Lowes, L., Mock, S., & Mosqueda, G. 2017. DesignSafe: A new cyberinfrastructure for natural hazards engineering. ASCE Natural Hazards Review, doi: 10.1061/(ASCE) NH. 1527-6996.0000246.

Rathje, E. M., Wang, Y., Stafford, P. J., Antonakos, G. & Saygili, G. 2014. Probabilistic assessment of the seismic performance of earth slopes. Bulletin of Earthquake Engineering, 12:1071–1090.

Rathje, E. M., & Antonakos, G. 2011. A unified model for predicting earthquake-induced sliding displacements of rigid and flexible slopes. Engineering Geology, 122(1): 51–60.

Rathje, E. M. & Saygili, G. 2009. Probabilistic assessment of earthquake-induced sliding displacements of natural slopes. Bulletin of the New Zealand Society for Earthquake Engineering, 42(1):18–27.

Saygili, G., Rathje, E. M. & Wang, Y. 2018. Probabilistic seismic hazard analysis for the sliding displacement of rigid sliding masses. DesignSafe-CI [publisher], Dataset, https://doi.org/10.17603/DS22D6K.

Saygili, G. & Rathje, E. M. 2008. Empirical predictive models for earthquake-induced sliding displacements of slopes. Journal of Geotechnical and Geoenvironmental Engineering, 134(6): 790–803.

Wang, Y. & Rathje, E. M. 2018. Application of a probabilistic assessment of the permanent seismic displacement of a slope. Journal of Geotechnical and Geoenvironmental Engineering, 144(6): doi:10.1061/(ASCE)GT.1943-5606.0001886.